Special Section on Transporters in Drug Disposition and Pharmacokinetic Prediction

Intravital Multiphoton Microscopy with Fluorescent Bile Salts in Rats as an In Vivo Biomarker for Hepatobiliary Transport Inhibition [S]

Jennifer Ryan, Ryan E. Morgan, Yuan Chen, Laurie P. Volak, Robert T. Dunn, II, and Kenneth W. Dunn

Division of Nephrology, Department of Medicine, Indiana University Medical Center, Indianapolis, Indiana (J.R., K.W.D.); Department of Comparative Biology and Safety Sciences, Department of Pharmacokinetics and Drug Metabolism, Amgen Inc., Thousand Oaks, California (R.E.M., Y.C., L.P.V., R.T.D.)

ABSTRACT

The bile salt export pump (BSEP) is expressed at the canalicular domain of hepatocytes, where it mediates the elimination of monovalent bile salts into the bile. Inhibition of BSEP is considered a susceptibility factor for drug-induced liver injury that often goes undetected during nonclinical testing. Although in vitro assays exist for screening BSEP inhibition, a reliable and specific method for confirming Bsep inhibition in vivo would be a valuable follow up to a BSEP screening strategy, helping to put a translatable context around in vitro inhibition data, incorporating processes such as metabolism, protein binding, and other exposure properties that are lacking in most in vitro BSEP models. Here, we describe studies in which methods of quantitative intravital microscopy were used to identify dose-dependent effects of two known BSEP/Bsep inhibitors, 2-[4-[4-(butylcarbamoyl)-2-[(2,4-dichlorophenyl)sulfonylamino]phenoxy]-3-methoxyphenyl]acetic acid (AMG-009) and bosentan, on hepatocellular transport of the fluorescent bile salts cholylglycyl amidofluorescein and cholyl-lysyl-fluorescein in rats. Results of these studies demonstrate that the intravital microscopy approach is capable of detecting Bsep inhibition at drug doses well below those found to increase serum bile acid levels, and also indicate that basolateral efflux transporters play a significant role in preventing cytosolic accumulation of bile acids under conditions of Bsep inhibition in rats. Studies of this kind can both improve our understanding of exposures needed to inhibit Bsep in vivo and provide unique insights into drug effects in ways that can improve our ability interpret animal studies for the prediction of human drug hepatotoxicity.

Introduction

Drug-induced liver injury is a leading cause of clinical trial failures and postmarketing drug withdrawals. The fact that drug-induced liver injury often goes undetected during nonclinical testing (Olson et al., 2000; Chen et al., 2015) suggests that the mechanisms of drug hepatotoxicity differ between humans and laboratory animals. For example, human hepatotoxicity is strongly associated with drugs that inhibit the bile salt export pump (BSEP), a transporter expressed at the canalicular domain of hepatocytes, with its primary function being the secretion of bile acids into the bile canaliculus (Stieger et al., 2007). In contrast, BSEP inhibitors generally show little or no evidence of liver injury in rodent studies (Fattinger et al., 2001; Funk et al., 2001a,b; Kostrubsky et al., 2003, 2006; Feng et al., 2009; Morgan et al., 2010, 2013). Examples of BSEP inhibitors associated with human

hepatotoxicity that have shown little or no evidence of liver injury during nonclinical testing include bosentan, 2-[4-[4-(butylcarbamoyl)-2-[(2,4-dichlorophenyl)sulfonylamino]phenoxy]-3-methoxyphenyl]acetic acid (AMG-009), and troglitazone (Fattinger et al., 2001; Funk et al., 2001b; Morgan et al., 2013).

There is genetic validation of BSEP as a target for toxicity in humans where mutations in the gene that encodes BSEP (ATP-binding cassette transporter, B11 or *ABCB11*) result in a complete loss of function and lead to a severe disease phenotype requiring liver transplantation during adolescence (Davit-Spraul et al., 2009). Bsep knockout mice, on the other hand, live a relatively normal life span, with only mild evidence of cholestasis (Wang et al., 2009). Some hypotheses as to the reasons that rodents appear less sensitive to hepatotoxicity due to Bsep inhibition include differences in the bile salt pool, bile salt metabolism, bile salt transporter expression, and others (Wang et al., 2009; Woodhead et al., 2014).

Given the strong association of human hepatotoxicity with drugs that inhibit BSEP and the fact that the liver injury seen in humans often goes undetected during nonclinical testing, a BSEP screening strategy is advised for the early detection of this putative liability. The challenge

ABBREVIATIONS: AMG-009, 2-[4-[4-(butylcarbamoyl)-2-[(2,4-dichlorophenyl)sulfonylamino]phenoxy]-3-methoxyphenyl]acetic acid; BSEP, bile salt export pump; CGamF, cholylglycyl amidofluorescein; CLF, cholyl-lysyl-fluorescein; DMSO, dimethylsulfoxide; Hoechst 33342, 2-(4-ethoxyphenyl)-6-[6-(4-methylpiperazin-1-yl)-1*H*-benzimidazol-2-yl]-1*H*-benzimidazole; MRP2, multidrug resistance-associated protein 2; NTCP, Na$^+$-dependent taurocholate cotransporting polypeptide.

with such a screening strategy is in translating in vitro measures of BSEP inhibition into predictions of in vivo effects. The practice of relating in vitro potencies to exposure values, such as concentration at steady state, has been shown to improve the correlation with hepatotoxicity outcome (Dawson et al., 2012; Morgan et al., 2013). However, the typical high-throughput BSEP transport assay uses membrane vesicles that overexpress the transporter, a simplistic system that lacks important components of in vivo exposure, such as metabolic capacity, uptake/efflux, and protein binding (van Staden et al., 2012). In the absence of a toxicologically relevant in vivo model that can recapitulate the BSEP-mediated liver injury seen in humans, an in vivo assay of Bsep function could aid in the translation of in vitro potencies to an in vivo response.

Although rats are not a toxicologically relevant model for Bsep-mediated hepatotoxicity, they can be used to confirm Bsep inhibition in vivo. Development of an assay of Bsep function in rats would provide a valuable follow up to a BSEP screening strategy, helping to put a translatable context around in vitro inhibition data, including in vivo exposure properties that are lacking in most in vitro BSEP models. Such an assay could be used to confirm the exposures needed to achieve in vivo BSEP inhibition and provide a better understanding of the relationship between in vitro data and in vivo outcome. Knowledge of the exposures needed to achieve in vivo Bsep inhibition would improve liver liability assessments by clarifying a margin of safety as compounds are advanced to human testing. Total plasma or serum bile acids have been used to confirm Bsep inhibition in rodents, but this method appears to lack sensitivity as will be shown in this work with AMG-009 and bosentan.

In previous studies, we have demonstrated that quantitative multiphoton microscopy can be used to quantify organic anion and bile acid transport in the liver of living rats at subcellular resolution (Babbey et al., 2012; Ryan et al., 2014; Dunn and Ryan, 2017). Here we extend this approach to assay transporter inhibition in rats, using cholylglycyl amidofluorescein (CGamF) and cholyl-lysyl-fluorescein (CLF) as fluorescent bile salt probes (de Waart et al., 2010; Kruglov et al., 2011). Quantitative intravital microscopy of fluorescent bile salt transport in the liver of living rats was used to identify acute, dose-dependent effects of AMG-009 and bosentan, two human and rat BSEP/Bsep inhibitors that have been associated with drug-induced liver injury in humans.

Materials and Methods

Reagents. Bosentan was purchased from Sequoia Research Products Limited (Pangbourne, United Kingdom). AMG-009 was synthesized at Amgen Incorporated (Thousand Oaks, CA). CGamF was purchased from WuXi AppTec (Tianjin, People's Republic of China), and CLF was purchased from Syncom (Groningen, the Netherlands). All other reagents were of the highest grade possible and acquired from readily available commercial vendors.

Dosing Solution Preparations. Bosentan and AMG-009 dosing solutions suitable for intravenous administration were prepared. Solutions of bosentan were prepared at 0.6, 2.0, and 6.0 mg/ml in 12.5% Captisol in distilled water, adjusted to pH 9.0 using NaOH, for dose levels of 3, 10, and 30 mg/kg, respectively. Solutions of AMG-009 were prepared at 0.6, 2.0, and 6.0 mg/ml in distilled water, adjusted to pH 9.0 using NaOH for dose levels of 3, 10, and 30 mg/kg, respectively.
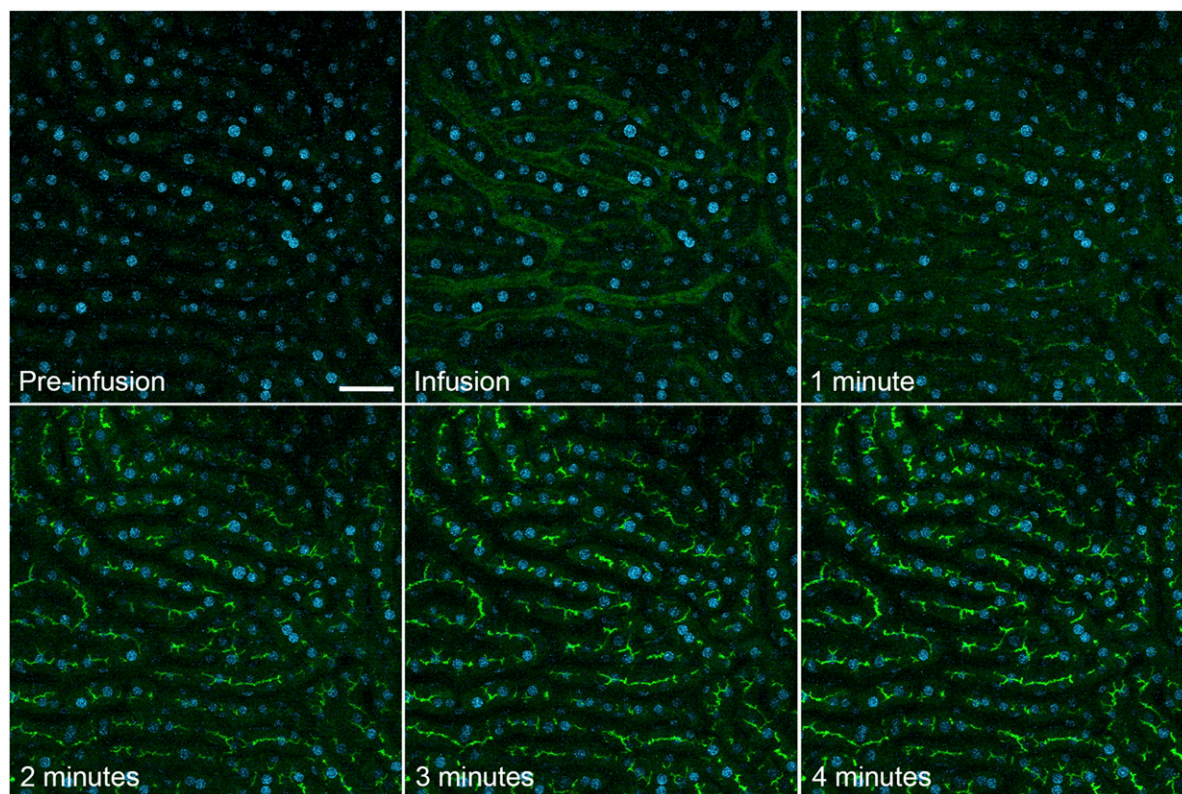

Fig. 1. Intravital microscopy of CGamF transport in the liver of a living rat. Intravital multiphoton microscopy was used to collect a series of fluorescence image volumes from the liver of a living rat after intravenous injection of 4 mg/kg CGamF. These image volumes were converted into a series of maximum projection (MIP) images for each time point, which are shown here. CGamF initially appearing in the sinusoids was rapidly transported, detectible in canaliculi as early as 1 minute after infusion, and subsequently increased in concentration over the next 3 minutes. The rat was injected with Hoechst 33342 (2 mg/kg) 30 minutes before imaging to label nuclei (blue). Scale bar is 50 μm in length.

CGamF powder was dissolved in dimethylsulfoxide (DMSO, 4 mg/50 μl), added to a solution of 0.5 N NaOH, which was then titrated to pH 7.0 using concentrated HCl to a final concentration of 4 mg/ml. CLF was dissolved in 0.9% saline to a concentration of 10 mg/ml. All experiments conducted for a particular test article were performed using the same batch of CGamF or CLF, with the dose adjusted to accommodate differences in fluorescence between batches so as to ensure hepatocyte labeling in the linear range of the microscope fluorescence detectors.

Animals for Intravital Microscopy Studies. Male Wistar rats (300–400 g) were purchased from Harlan Laboratories (Indianapolis, IN) and housed in pairs in the Indiana University School of Medicine Laboratory Animal Resource Center. The rats were maintained on a diet of Teklad 4% mouse/rat diet (Envigo RMS, Indianapolis, IN) and water ad libitum. An acclimatization interval of at least 4 days was allowed before the performance of any experiments. All animal experiments were approved and conducted according to the Institutional Animal Care and Use Committee guidelines of Indiana University, and adhered to the guide for the care and use of animals (NRC, 2011).

Intravital Microscopy Studies of Fluorescent Bile Salt Transport. Fluorescent bile salt transport was characterized using intravital multiphoton microscopy, using an approach similar to that previously applied (Babbey et al., 2012; Ryan et al., 2014) and described in detail elsewhere (Dunn and Ryan, 2017). Multiphoton microscopy was conducted with an Olympus Fluoview 1000 MPE confocal/multiphoton microscope system (Olympus, Tokyo, Japan) mounted on an Olympus IX-81 inverted stand, using an Olympus 25X, NA1.05 water immersion objective, with 830 nm excitation provided by a Mai Tai DeepSee laser (Spectra-Physics, Santa Clara, CA). Fluorescence emissions were collected in three nondescanned photomultiplier detectors: blue channel (380–480 nm), green channel (500–550 nm), and red channel (560–650 nm).

Rats were sedated with 5% isoflurane and weighed; and 130 mg/kg Inactin (Sigma-Aldrich, St. Louis, MO) was administered intraperitoneally for anesthesia. During surgery, the rats were placed on a heating pad to maintain body temperature, which was monitored using a rectal thermometer. Once anesthetized, a 3 × 1.5 cm L-shaped incision was made 1 cm right of ventral midline in the neck. A jugular cannula was then placed using PE 50 tubing, filled with sterile 0.9% saline, and attached to a Luer stub adapter and 1 ml syringe; the neck was
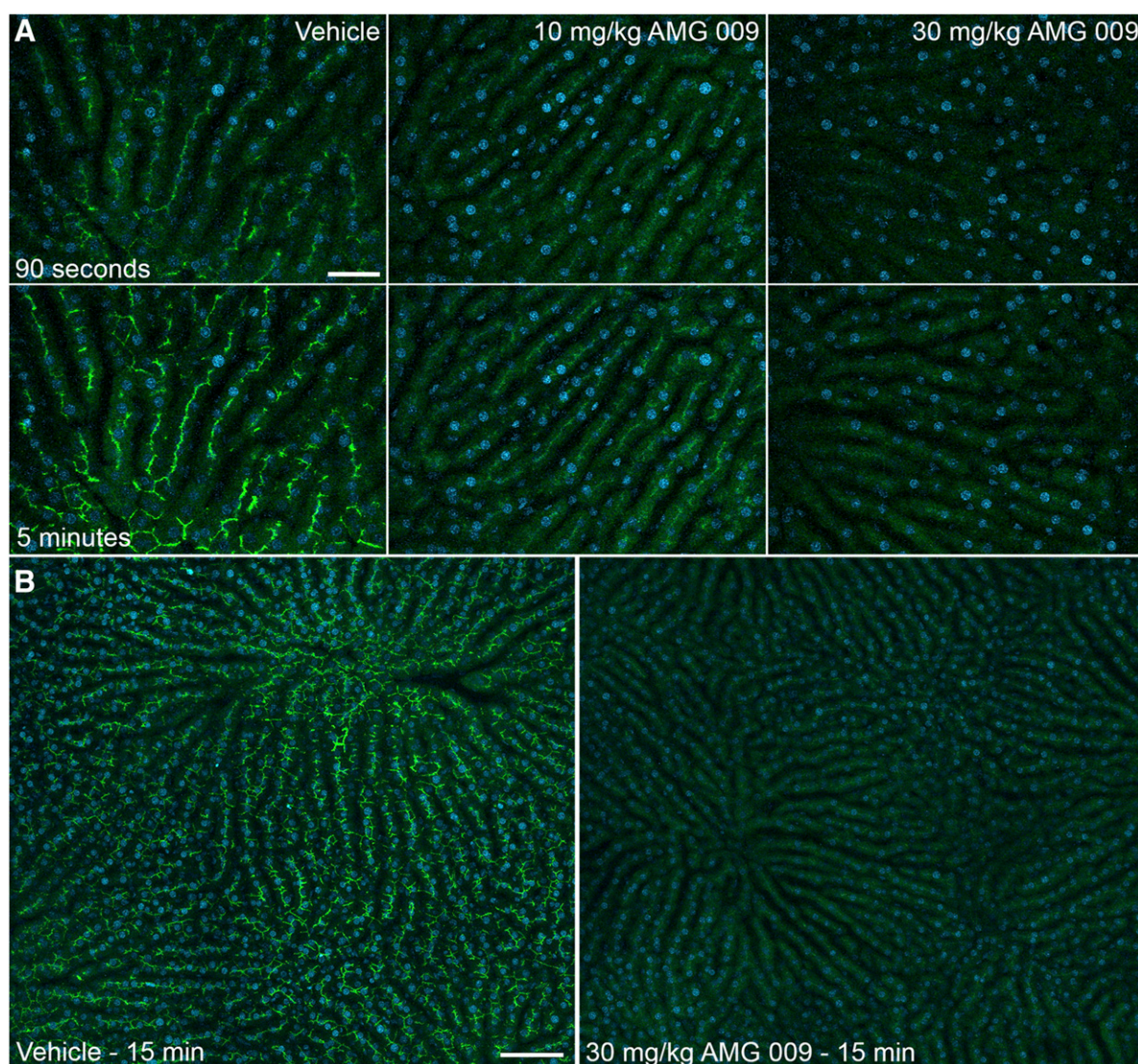
Fig. 2. Effects of AMG-009 on CGamF transport in rat liver. (A) Time course of CGamF transport in the livers of living rats 20 minutes after intravenous injection with vehicle (left), 10 mg/kg AMG-009 (middle), or 30 mg/kg AMG-009 (right). Top row: projected images collected 90 seconds after infusion of CGamF. Bottom row: projected images collected 5 minutes after infusion of CGamF. The time-series of maximum projection (MIP) images collected over 5 minutes after intravenous injection in rats treated with vehicle or 30 mg/kg AMG-009 is shown in an accompanying video (Supplemental Video 1) (at ~100× speed). (B) Mosaics assembled from nine adjacent volumes collected 12–15 minutes after intravenous injection of CGamF for a rat treated with vehicle (left) or 30 mg/kg AMG-009 (right). Scale bars are 50 μm (A) or 100 microns (B) in length.
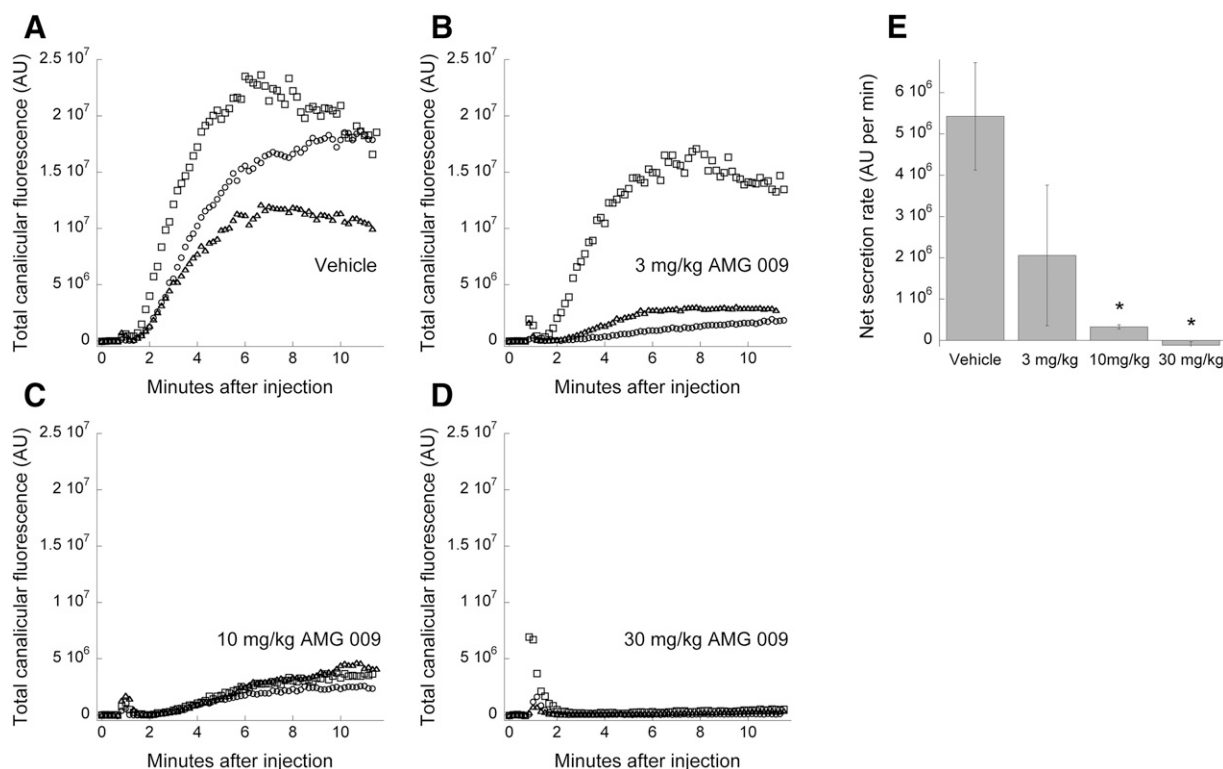
Fig. 3. In vivo dose-dependent inhibition of canalicular secretion by AMG-009 in rats. Kinetics of canalicular secretion of CGamF for individual rats treated with (A) vehicle, (B) 3 mg/kg AMG-009, (C) 10 mg/kg AMG-009, or (D) 30 mg/kg AMG-009. In each graph measurements are shown for each of three replicate rats. (The small spike in fluorescence at 1 minute is an artifact of the segmentation procedure, which detects a small fraction of the sinusoid fluorescence during infusion.) (E) Summary of effects on CGamF net secretion rate (linear rate of initial secretion) (mean ± S.E.M.). *$P < 0.05$, Dunnett's multiple comparison procedure. For all conditions, $n = 3$.

sutured with 3-0 black silk sterile suture. At this time, a 2-mg/kg bolus of 2-(4-ethoxyphenyl)-6-[6-(4-methylpiperazin-1-yl)-1*H*-benzimidazol-2-yl]-1*H*-benzimidazole (Hoechst 33342; Invitrogen/Life Technologies, Carlsbad, CA) diluted in 0.9% sterile saline to a total 0.4 ml was injected into the jugular line to label cell nuclei.

To expose the liver for imaging, a ventral 4-cm incision was made across the torso 1 to 2 cm below the middle of the rib cage. A wet (0.9% saline) 2×2 gauze sponge was gently placed below the left lateral liver lobe. The liver was secured to the bottom of a Willco coverslip-bottomed dish (GWST-5040; Warner Instruments, Hamden, CT) via cyanoacrylate gluing of the gauze below the liver to the plate or by gluing the liver itself to the plate. Sterile 0.9% saline was then placed in the coverslip-bottomed dish to keep the liver moist throughout the imaging session.

A small dose of CGamF or CLF was administered intravenously to identify a field of hepatocytes for analysis. Rats were then injected intravenously with AMG-009, bosentan, or vehicle in a volume of 5 ml/kg. The rats were placed ventral side down on the stage of an inverted microscope, with heating pads placed below the rats to warm the stage. A heater was used to warm the objective lens, and another heating pad was placed over each rat before imaging. To prevent movement during imaging, the rats' hind legs and the glass-bottom plate were taped securely to the stage.

An appropriate field of the liver was identified, and at a time point 20 minutes after administration of test article, a series of image volumes (six focal planes, spaced 1 micron apart) were then collected continuously just before and for 12 minutes after intravenous injection of CGamF or CLF (0.4–4.0 and 0.5 mg/kg, respectively). A high-resolution mosaic, consisting of nine contiguous volumes (each consisting of 15 planes, spaced 1 micron apart) was then collected.

Quantitative Digital Image Analysis. Quantitative image analysis was conducted using MetaMorph image processing software (Molecular Devices, Downington, PA). To ensure sequential capture of images of the canaliculi despite residual vertical motion of the liver, three-dimensional image volumes were collected at each time point. Each of these volumes were then projected into a single, maximum-projection image (Babbey et al., 2012; Ryan et al., 2014), which

was used for quantitative analysis. This procedure had the effect of ensuring collection of images of the same set of canaliculi throughout the time series.

Canalicular fluorescence was quantified as follows. To eliminate crosstalk of the nuclear Hoechst fluorescence into the CGamF/CLF fluorescence channel, projections of images collected with the blue channel (380–480 nm) were subtracted from the corresponding projected images of the green channel (500–550 nm). A series of binary masks of the canalicular regions were generated by applying a high-pass filter to each time-point projection (subtracting a large-neighborhood (24 pixel square) median filter from each (Maxfield and Dunn, 1990), from which single pixels were then eliminated. The effectiveness of this approach is demonstrated in supplementary data (Supplemental Fig. 1). Canalicular fluorescence for each time point was quantified as the integrated green channel signal occurring in the corresponding masked region. Fluorescence measurements were corrected for background by subtracting the mean signal during the five time points preceding the appearance of CGamF/CLF in the sinusoids. Net canalicular secretion rates were quantified as the linear slope of the background-corrected measurements obtained from the regions under the canalicular mask during the initial interval of canalicular uptake (typically 1 minute after infusion, ~2 minutes after injection).

To quantify mean cytosolic fluorescence, a series of masks of nuclear regions were created by binarizing projections of the images collected in the blue channel (380–480 nm) for each time point. Cytosolic regions were then identified as regions surrounding the nuclear masks, located in 2-pixel-wide lines, 6 pixels away from the nucleus boundary, after subtraction of the corresponding canalicular mask. Mean cytosolic fluorescence for each time point was quantified as the mean green channel signal occurring in the cytosolic regions. Plotted values were corrected for background by subtracting the mean signal measured in the regions during the five time points preceding the appearance of CGamF/CLF in the sinusoids. Cytosolic uptake rates were quantified as the linear slope over the initial interval of cytosolic uptake (starting immediately upon infusion, typically 1 minute after injection).

Mosaics were assembled from individual volumes by projecting each volume into a single projection image and then aligning and assembling the projections into a single image using Adobe Photoshop (Adobe Systems, Mountain View,
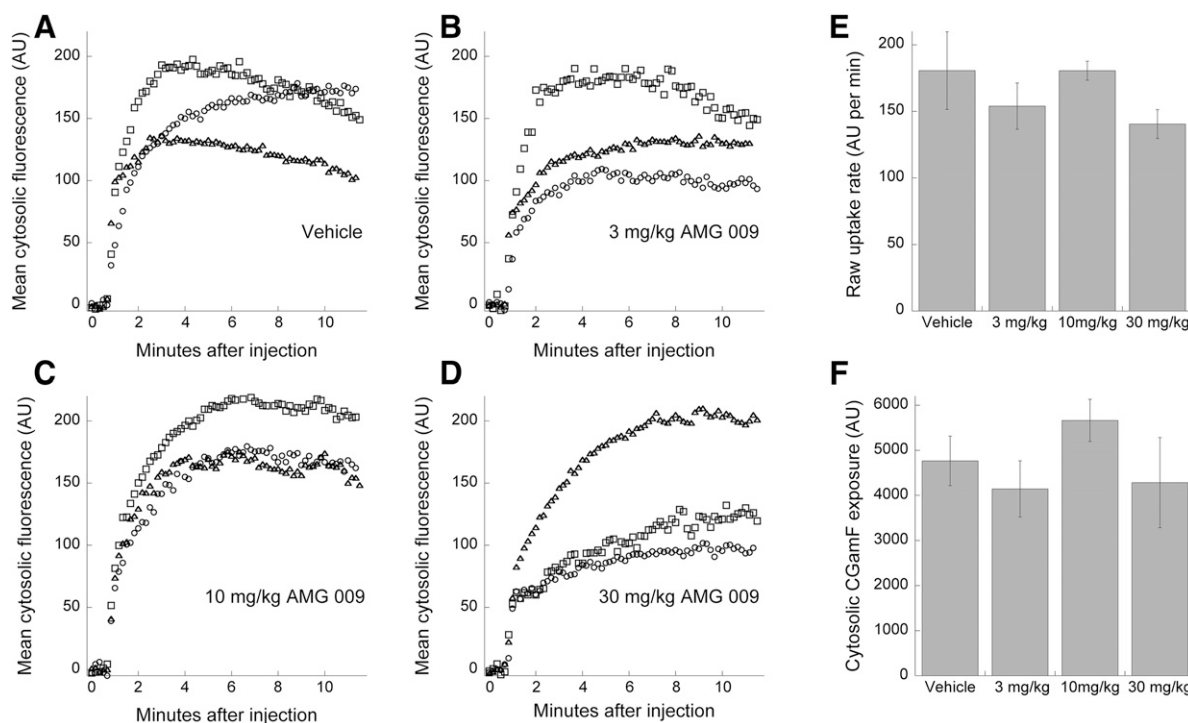
Fig. 4. Quantification of the in vivo effects of AMG-009 on hepatocellular CGamF uptake. Kinetics of CGamF cytosolic uptake for individual rats treated with (A) vehicle, (B) 3 mg/kg AMG-009, (C) 10 mg/kg AMG-009, or (D) 30 mg/kg AMG-009. In each graph measurements are shown for each of three replicate rats. (E) Summary of effects on CGamF net uptake (linear rate during initial uptake). (F) Cumulative cytosolic CGamF fluorescence, measured from 6 to 11 minutes after CGamF injection (mean ± S.E. M.). For all conditions, $n = 3$.

CA). Canalicular and cytosolic fluorescence in the mosaics were quantified as described earlier, and standardized to a common field size to compensate for small differences in the size of the resulting mosaics.

Measurement of Serum Total Bile Acids from Rats Exposed to AMG-009 or Bosentan. Biochemical analyses of the effects of drugs on serum bile acid levels were conducted using male Sprague-Dawley rats which, like the Wistar rats used in the microscopy studies, have been extensively used in Bsep inhibitor studies (Fattinger et al., 2001; Kostrubsky et al., 2003; Leslie et al., 2007; Morgan et al., 2013) and have been found to show a similar sensitivity to bosentan (Fouassier et al., 2002). Rats approximately 10 weeks of age were purchased from Charles River Laboratories (Wilmington, MA) and allowed at least 1 week to acclimate. All animals were group housed (two or three per cage) at an Association for Assessment and Accreditation of Laboratory Animal Care International accredited facility in nonsterile, ventilated microisolator housing. The research protocols were approved by the institutional animal care and use committee. Animals were given ad libitum access to pelleted feed and purified, municipal water. The 12-hour light/dark cycle had controlled temperature and humidity. Animals were given access to enrichment opportunities. Animals were fasted 2 to 3 hours before the administration of a single intravenous dose of either AMG-009 (Amgen study 111327) or bosentan (Amgen study 118507), and food was returned after the final bleed before the 24-hour time point (2–6 hours after dose administration). Animals were again fasted 2 to 3 hours before the terminal 24-hour bleed.

The formulations and dosing volumes were as described under the dosing solution preparations section. For the Amgen serum total bile acid studies, 0, 10, 30, and 100 mg/kg dose levels were evaluated for AMG-009 or bosentan. For the AMG-009 study, six animals were assigned to each dose group where the first three animals in each group were bled at 5, 30, 60, and 360 minutes after dose administration (terminal bleed at 360 minutes after dose administration), and the second three animals in each group were bled at 15, 45, 120, and 1440 minutes after dose administration. Plasma was collected for exposure analysis at each time point, and serum was collected for total bile acid analysis. Total bile acids were measured using an enzymatic, colorimetric assay for total bile acids from BioQuant (catalog number BQ092A-EALD; San Diego, CA) and a Tecan Safire plate reader (540 nm wavelength; Tecan Group, Männedorf, Switzerland).

In the bosentan studies, there were 10 animals per dose group. The first five animals in each group were bled at 5, 30, 120, and 1440 minutes after dose administration, and the second five animals per dose group were bled at 15, 60, 360, and 1440 minutes after dose administration. Plasma was collected for exposure analysis at each time point, and serum was collected for total bile acid analysis. Total bile acids were measured using the BioQuant assay described earlier; however, the analysis was performed on a AU400 chemistry analyzer (Beckman Coulter, Brea, CA).

Analysis of Rat Plasma Samples. In the intravital imaging studies conducted at Indiana University Medical Center, plasma samples were collected in lithium heparin tubes 50 minutes after the intravenous dose of AMG-009 or bosentan, stored at approximately 70°C, and shipped on dry ice to Amgen for exposure analysis. Briefly, plasma was analyzed by liquid chromatography mass spectrometry using multiple reaction monitoring in positive ionization mode. The lower limit of quantitation for both AMG-009 and bosentan in the assay was 100 μg/l. Verapamil was used as an internal standard. The bioanalytical and toxicokinetic analyses were performed in Watson LIMS software (Thermo Fisher Scientific, Waltham, MA).

To estimate the maximum concentration (C_{max}) achieved after a single bolus intravenous dose of AMG-009 or bosentan in male rats from the 50-minute postdose samples collected during the intravital studies, exposure data from previously conducted intravenous studies (Amgen studies 111327 and 118507) were compared with the intravital exposure values. For the previous AMG-009 study (111327), the plasma concentrations for individual animals at the 45-minute time point were plotted against C_{max}. In this study, three animals per dose group were bled at 15, 45, 120, and 1440 minutes after dose administration or at 5, 30, 30, and 360 minutes after dose administration. Linear regression of the plasma concentration at 45 minutes after dose administration versus C_{max} was performed, resulting in the equation $y = 0.571x$, where y is the plasma concentration and x is the estimated C_{max}. The intravital plasma concentrations at 50 minutes after dose administration were then substituted for y to generate an estimated C_{max}.

Similarly, for the previous bosentan study (118507), five animals per dose group were bled at 5, 30, 120, and 1440 minutes after dose administration, or at 15, 60, 360, and 1440 minutes after dose administration. Linear regression of the plasma concentrations at the 30- and 60-minute time points versus C_{max} was

TABLE 1
Summary of intravital microscopy measurements

For all conditions n = 3, except the 3 mg/kg bosentan treatment group (CGamF studies) for which one animal was omitted due to lack of detectable bosentan in plasma, and the 9-field integrated CGamF measures in vehicle-treated rats in the AMG-009 studies for which mosaics were collected for only two rats.

Compound Dose	Net Canalicular Secretion Rate (AU/min)		9-Field Canalicular Fluorescence (AU)	Cytosolic Uptake Rate (AU/min)		Cumulative Cytosolic Exposure (AU)		9-Field Cytosolic Fluorescence (AU)
	CGamF	CLF	CGamF	CGamF	CLF	CGamF	CLF	CGamF
AMG-009								
Vehicle	5.426e+06 ± 1.301e+06	2.104e+07 ± 6.176e+06	1.1870e+08 ± 5.321e+07	180.7 ± 29.17	135.9 ± 7.217	4765 ± 550.3	2787.8 ± 505.4	587.5 ± 21.50
3 mg/kg	2.057e+06 ± 1.701e+06	ND	4.455e+07 ± 1.457e+07	154.0 ± 17.42	ND	4143 ± 623.2	ND	598.3 ± 24.29
10 mg/kg	3.273e+05 ± 52,250[a]	ND	2.873e+07 ± 7.516e+06[a]	180.6 ± 7.160	ND	5663 ± 469.5	ND	662.0 ± 18.58
30 mg/kg	−1.1612e+05 ± 82,430[a]	27,870 ± 25,380[a]	2.733e+06 ± 7.694e+05[a]	140.5 ± 10.86	68.90 ± 14.95[a]	4283 ± 1000.	3450 ± 897.6	568.7 ± 13.67
Bosentan								
Vehicle	1.238e+07 ± 1.816e+06	1.622e+07 ± 1.189e+06	1.839e+08 ± 3.380e+07	248.80 ± 22.96	143.40 ± 7.538	5007 ± 450.7	2809 ± 164.9	512.0 ± 12.70
3 mg/kg	9.950e+06 ± 1.453e+06	ND	1.687e+08 ± 4.719e+07	148.90 ± 58.61	ND	2882 ± 412.9	ND	470.0 ± 3.000
10 mg/kg	6.854e+06 ± 6.057e+05[a]	ND	1.120e+08 ± 2.719e+06	137.6 ± 31.12	ND	3878 ± 993.2	ND	474.0 ± 5.292
30 mg/kg	2.555e+06 ± 9.804e+05[b]	4.681e+06 ± 2.182e+06[b]	1.039e+08 ± 1.180e+07	128.5 ± 7.611[a]	57.62 ± 10.75[b]	5110 ± 623.4	3683 ± 489.7	503.7 ± 14.35

ND, not determined.
[a]$P < 0.05$, Dunnett's multiple comparison, Student's t test for single comparisons.
[b]$P < 0.01$, Dunnett's multiple comparison, Student's t test for single comparisons.

performed, resulting in the equation $y = 0.710x$, where y is the plasma concentration and x is the estimated C_{max}. The intravital plasma concentrations at 50 minutes after dose administration for the bosentan-treated animals were then substituted for y to establish an estimated C_{max}.

In Vitro Functional Transport Assessments in Membrane Vesicles Overexpressing Rat Bsep or Mrp2. Inverted membrane vesicles created from Sf9 insect cells overexpressing rat Bsep or multidrug resistance-associated protein 2 (Mrp2) (catalog numbers GM0006 and GM0002, respectively) were purchased from Life Technologies (Grand Island, NY). Radioactive substrates for the membrane vesicle assays, ^{3}H-taurocholate (^{3}H-T) for Bsep and ^{3}H-estradiol-17β-D-glucuronide (^{3}H-E$_2$17βG) for Mrp2, were purchased from PerkinElmer (Waltham, MA). All other reagents and buffers for the membrane vesicle assays were of the highest grade possible and were exactly as described in van Staden et al. (2012).

The transporter methods and data analyses performed in the present work were also exactly as described in van Staden et al. (2012), but the membrane vesicles were for the rat versions of Bsep and Mrp2. Briefly, rat Bsep (25 μg membrane vesicle protein per reaction) or Mrp2 (50 μg membrane vesicle protein per reaction) membrane vesicles were incubated with a radiolabeled substrate in the presence or absence of 4 mM ATP. The absence of ATP served as the negative control, and the resulting radioactivity when exposed to vehicle alone (1.3% DMSO) was considered background or noise. The with-ATP controls and 1.3% DMSO represented true signal. For the rat Mrp2 assay, 2 mM glutathione was added to the reaction. The Bsep assay was performed at room temperature, with an incubation time of 15 to 20 minutes. The Mrp2 assay was performed at 37°C, with an incubation time of 20 minutes. AMG-009 or bosentan were evaluated at 10 concentrations, diluted in one-third increments, spanning 0–133 μM. Nonlinear regression analysis was performed, and IC_{50} values were generated as an estimate of potency as described previously elsewhere (Morgan et al., 2010; van Staden et al., 2012).

Additional experiments were conducted to evaluate the in vitro transport of CGamF or CLF in rat Bsep or Mrp2 membrane vesicles. These experiments were conducted exactly as described previously, but no radioactive substrates were added to the reactions. The transport of CGamF or CLF was tested at 0–133 μM, 10 concentrations per fluorescent probe, diluted in one-third increments and in the presence of 4 mM ATP. As performed in the radioactivity-based assays described earlier, the with- or without-ATP controls represented maximum signal or background fluorescence, respectively. After the filter plates were washed 4 times with cold washing buffer and air dried, 100 μl of 0.1 N NaOH was used to lyse the membrane vesicles. The lysates were collected via vacuum filtration into collection plates, and the fluorescence measured at an excitation of 490 nm, and an emission of 525 nm using a Tecan Infinite plate reader (Tecan Group).

Figure Preparation. Quantitative analysis was conducted on raw image data, but micrograph images were both contrast enhanced (resetting minimum and maximal values, and adjusting gamma to 1.2) and smoothed using a Gaussian filter. In the color images, the visibility of Hoechst-labeled nuclei was enhanced by selectively adjusting the hue, saturation, and lightness of the blue channel. In all cases, the images to be compared were processed identically to one another and in such a way that the processing preserved the visibility of both the dim and bright structures of the original image. Images were processed, assembled into figures and annotated using Adobe Photoshop (Adobe Systems). Graphics were produced and summary statistics obtained using Kaleidagraph (Synergy Software, Reading, PA).

Preparation of Videos. MPEG videos were prepared using the TMPGEnc 2.5 video encoder (Pegasys, Tokyo, Japan) from uncompressed AVI files prepared in MetaMorph (Molecular Devices).

Results

Intravital Microscopy of CGamF Hepatocellular Transport in Rats. The metabolism and transport of CGamF have been previously shown to be similar to that of native bile salts in rats (Holzinger et al., 1997) and in perfused rat livers (Holzinger et al., 1998). Studies of transfected cells have demonstrated that CGamF is a substrate for human Na$^+$-dependent taurocholate cotransporting polypeptide (NTCP) and BSEP (Mita et al., 2006) and for rat Ntcp (Boyer et al., 1994). Studies of cultured rat hepatocytes have demonstrated that Bsep expression is
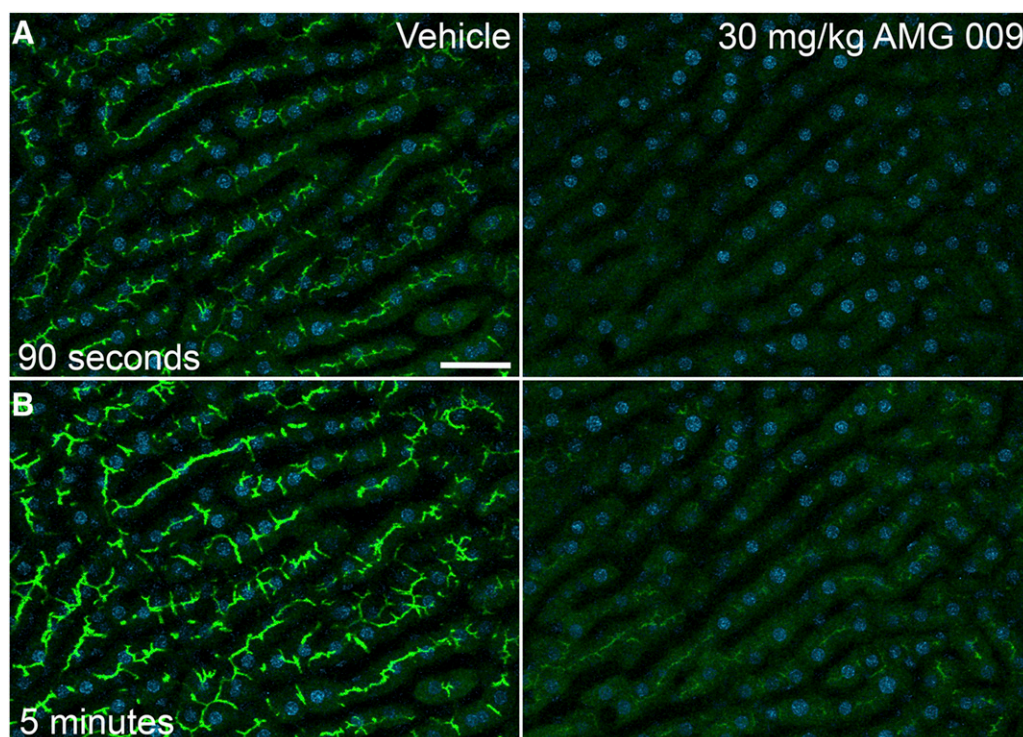
Fig. 5. Effects of AMG-009 on CLF transport in rat liver. Time course of CLF transport in the livers of living rats 20 minutes after intravenous injection with vehicle (left) or 30 mg/kg AMG-009 (right). The time-series of maximum projection (MIP) images collected over 5 minutes after intravenous injection in rats treated with vehicle or 30 mg/kg AMG-009 is shown in an accompanying video (Supplemental Video 2) (at ~100× speed). Scale bar is 50 μm in length.

required for CGamF secretion (Kruglov et al., 2011). Our studies of inverted membrane vesicles created from Sf9 insect cells overexpressing rat Bsep or Mrp2 demonstrate that CGamF is transported by both Bsep and, to a lesser extent, Mrp2 in an ATP-dependent manner (Supplemental Fig. 2).

Figure 1 shows a time series of multiphoton fluorescence excitation images collected from a 364 × 364 micron region of the liver of a living rat after intravenous injection of CGamF. Nuclei were labeled (blue) by intravenous injection of Hoechst 33342 30 minutes before imaging. These images demonstrate that CGamF (green fluorescence) is rapidly transported from sinusoids to bile canaliculi, with detectible fluorescence appearing in canaliculi within a minute of infusion and subsequently increasing in intensity over the next 3 minutes.

Intravital Microscopy of the Effects of AMG-009 on CGamF Hepatocellular Transport in Rats. To evaluate the effect of AMG-009 on hepatic bile salt transport, the same approach was used to characterize CGamF transport in rats 20 minutes after intravenous administration of 3, 10, or 30 mg/kg AMG-009 or vehicle. Figure 2A shows that detectible amounts of CGamF are found in canaliculi within 90 seconds of infusion in a vehicle-treated rat, subsequently increasing in brightness over the next 3.5 minutes. In contrast, transport of CGamF into canaliculi is slowed or blocked completely in rats treated with either 10 or 30 mg/kg AMG-009, respectively. The inhibitory effect of AMG-009 on CGamF transport is also demonstrated in the complete 8-minute series of images shown in an accompanying video (Supplemental Video 1), which shows that the rapid canalicular transport observed in a vehicle-treated rat is completely absent in a rat treated with 30 mg/kg AMG-009.

These studies were repeated for three rats per treatment, and digital image analysis was used to quantify canalicular fluorescence over time (Fig. 3, A–D). The results of these studies show that canalicular transport of CGamF was essentially blocked in rats treated with 10 or 30 mg/kg, and in two of three rats treated with 3 mg/kg AMG-009. It is uncertain

why one animal in the 3 mg/kg group did not respond because the AMG-009 exposure for this animal was similar to that achieved in the other two. The rates of net secretion, measured as the linear rate of change in canalicular fluorescence during the initial secretion period, demonstrate that the rate of canalicular transport of CGamF is significantly reduced 20 minutes after treatment with 10 or 30 mg/kg AMG-009 (Fig. 3E).

To evaluate the effects of AMG-009 on CGamF hepatocellular uptake, we measured the change in mean cytosolic fluorescence over time for each animal. These quantifications showed similar initial rates of increase for all treatment conditions, although the peak cytosolic fluorescence varied between and within each treatment (Fig. 4, A–D). Quantification of uptake rates (measured as the linear rate of change in mean cytosolic fluorescence during the initial uptake period) showed that AMG-009 had no significant effect on the CGamF uptake rate (Fig. 4E). These results support the conclusion that AMG-009 inhibits CGamF transport into the bile by blocking canalicular secretion.

In the presence of unimpeded uptake (i.e., Ntcp inhibition), one would expect that AMG-009 doses that block secretion would induce significant cytosolic accumulation of CGamF. Surprisingly, the measurements of cytosolic fluorescence shown in Fig. 4, A–D, indicate no such effect. Quantifications of cytosolic CGamF exposure (measured as cumulative cytosolic fluorescence over the period from 6 to 11 minutes after injection) likewise indicate that inhibition of canalicular CGamF secretion by AMG-009 was not accompanied by a corresponding increase in cytosolic CGamF levels (Fig. 4F).

Although it was not possible to characterize the kinetics in more than one field for each animal, the behaviors of the single fields were essentially reproduced in 9-field mosaics that were collected from the surrounding regions 12–15 minutes after probe administration (Fig. 2B). These mosaics, representing ~1 × 1 mm regions encompassing several lobules, consistently demonstrated that the behaviors of the single fields used for kinetic analysis were representative of larger regions, and also

demonstrated that their function was not significantly impacted by repeated imaging. Quantifications of total canalicular fluorescence in these mosaics supported the kinetic analyses, demonstrating that AMG-009 significantly reduced the total amount of canalicular CGamF at doses of 10 and 30 mg/kg but had no effect on mean levels of CGamF fluorescence in hepatocyte cytosols (Table 1).

Intravital Microscopy of the Effects of AMG-009 on CLF Hepatocellular Transport in Rats. The effects of AMG-009 on hepatic transport were also evaluated using the fluorescent probe CLF, which is frequently used to assay hepatocellular transport (Swift et al., 2010; Letzsch et al., 2015). Although studies of transfected cells suggest that biliary secretion of CLF is mediated by MRP2 in humans (de Waart et al., 2010), studies of wild-type and Mrp2-deficient TR$^-$ rats indicate that CLF secretion is mediated by Bsep in rats (Mills et al., 1997, 1999). Our studies of inverted membrane vesicles created from Sf9 insect cells overexpressing rat Bsep or Mrp2 demonstrate that CLF is transported by both Bsep and Mrp2 in an ATP-dependent manner in vitro (Supplemental Fig. 2).

Similar to results obtained with CGamF, treatment of rats with 30 mg/kg AMG-009 blocked secretion of CLF into bile canaliculi (Figs. 5; Fig. 6A), significantly reducing the rate of net secretion (Fig. 6B; Table 1). The effect of AMG-009 was demonstrated in the complete 8-minute series of images shown in an accompanying video (Supplemental Video 2), which shows that, like CGamF, the rapid canalicular transport of CLF observed in a vehicle-treated rat is completely absent in a rat treated with 30 mg/kg AMG-009. Whereas AMG-009 had no effect on CGamF uptake, treatment of rats with 30 mg/kg AMG-009 significantly inhibited CLF uptake, reducing the initial rate of uptake by more than 50% (Fig. 6, C and D). Although the kinetics of cytosolic CLF
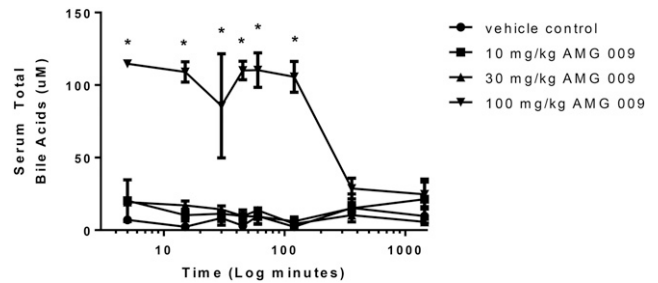

Fig. 7. Serum total bile acids in rats after a single intravenous dose of AMG-009. Serum total bile acid levels in rats treated intravenously with vehicle, 10, 30, or 100 mg/kg AMG-009 over a 24-hour time course. Three rats per time point, per dose group. Symbols represent mean values at each time point, and bars are S.E.M. *Dunnett's post hoc comparison, $P < 0.05$ (performed in GraphPad Prism 7; GraphPad Software, San Diego, CA).

fluorescence suggest that AMG-009 increases cytosolic exposure to CLF, differences in cumulative cytosolic fluorescence, measured from 6 to 11 minutes after infusion, were not statistically significant (Table 1).

Effects of AMG-009 on Plasma Bile Acid Levels. Serum samples were collected from rats over a 24-hour period after intravenous injection of vehicle or 10, 30, or 100 mg/kg AMG-009 and analyzed for total bile acids. As shown in Fig. 7, treatment of animals with 10 and 30 mg/kg had no detectable effect on serum bile acid levels, whereas a dose of 100 mg/kg resulted in a statistically significant elevation of total serum bile acids from 5 to 120 minutes after dose administration. Bile acids then returned to vehicle control values by 360 and 1440 minutes after dose administration.
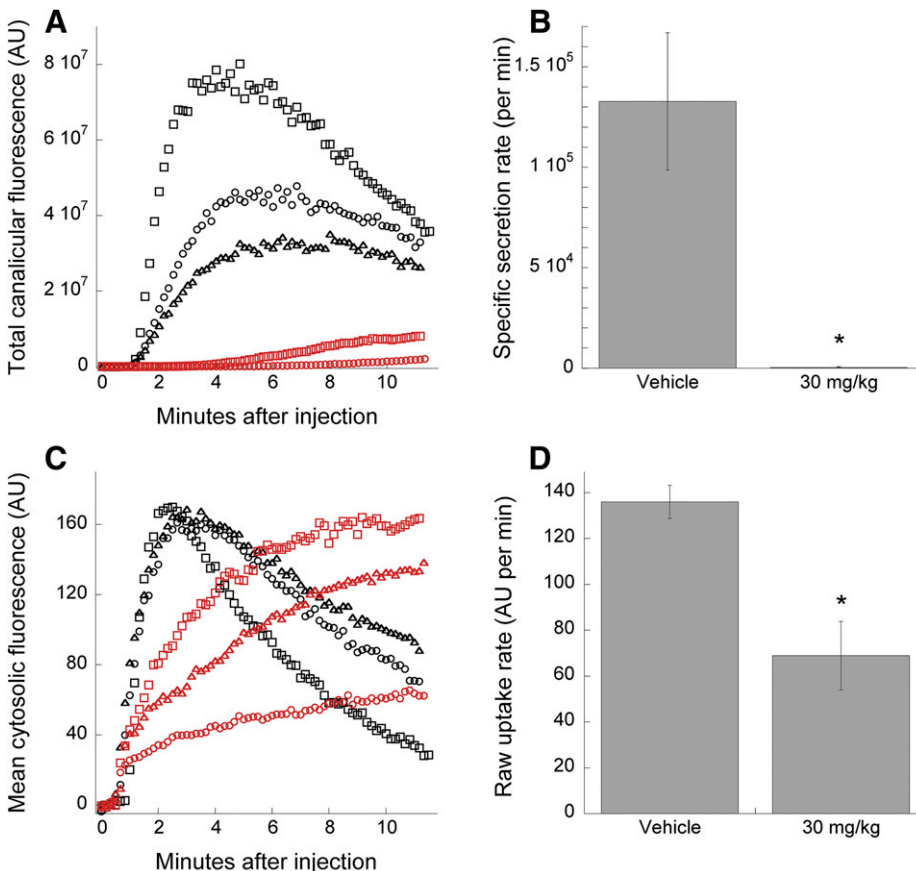
Fig. 6. Quantification of the effects of AMG-009 on CLF transport in vivo. (A) Kinetics of CLF canalicular secretion for individual rats treated with vehicle (black symbols) or 30 mg/kg AMG-009 (red symbols). Measurements are shown for each of three replicate rats for each condition. (B) Summary of effects on rates of CLF net secretion (linear rate of initial secretion) (mean ± S.E.M.). (C) Kinetics of cytosolic CLF uptake for individual rats treated with vehicle (black symbols) or 30 mg/kg AMG-009 (red symbols). Measurements are shown for each of three replicate rats for each condition. (D) Summary of effects on net CLF uptake (linear rate during initial uptake) (mean ± S.E.M.). *$P < 0.05$, Student's t test. For all conditions, $n = 3$.
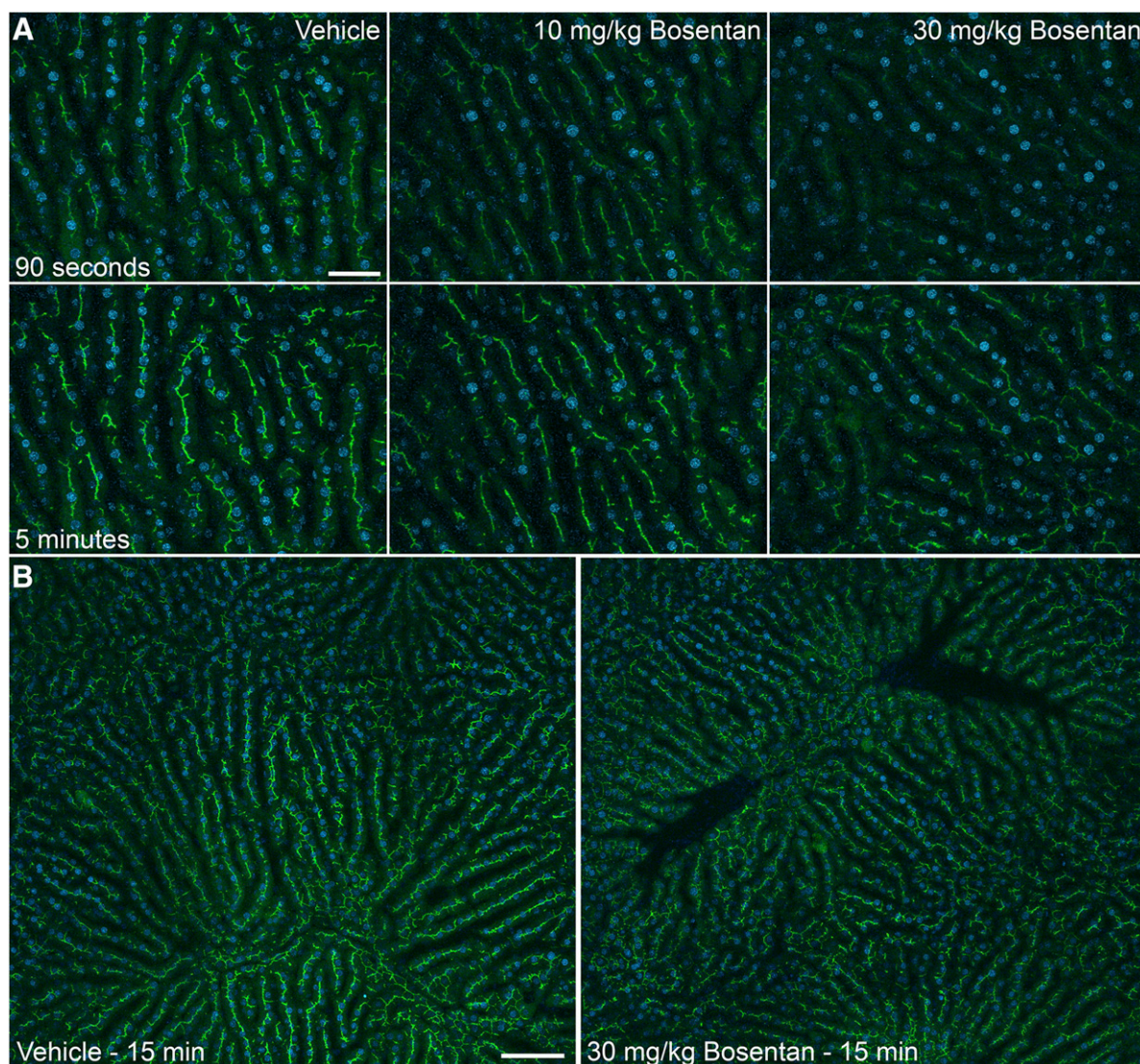
Fig. 8. Effects of bosentan on CGamF transport in rat liver. (A) Time course of CGamF transport in the liver of living rats 20 minutes after intravenous injection with vehicle (left), 10 mg/kg bosentan (middle), or 30 mg/kg bosentan (right). Top row: projected images collected 90 seconds after CGamF infusion. Bottom row: projected images collected 5 minutes after CGamF infusion. The time-series of maximum projection (MIP) images collected over 5 minutes after intravenous injection in rats treated with vehicle or 30 mg/kg bosentan is shown in an accompanying video (Supplemental Video 3) (at ~100× speed). (B) Mosaics assembled from nine adjacent volumes collected 12–15 minutes after intravenous injection of CGamF for a rat treated with vehicle (left) or 30 mg/kg bosentan (right). Scale bars are 50 μm (A) or 100 microns (B) in length.

Intravital Microscopy of the Effects of Bosentan on CGamF Hepatocellular Transport in Rats. Similar studies were conducted in rats treated with 3, 10 or 30 mg/kg bosentan, another Bsep inhibitor that has been associated with liver injury in humans (Fattinger et al., 2001). The effects of bosentan on CGamF canalicular secretion were similar to those observed in the studies with AMG-009 (Fig. 8A; Fig. 9), with significant decreases in the rates of net secretion apparent at both 10 and 30 mg/kg doses (Fig. 9E). This inhibitory effect is also demonstrated in the complete 8-minute series of images shown in an accompanying video (Supplemental Video 3), which shows that the rapid canalicular transport observed in a vehicle-treated rat is significantly inhibited in a rat treated with 30 mg/kg bosentan. Evaluations of the 9-field mosaics (Fig. 8B) indicated that the results obtained in the kinetic studies of individual fields were generally representative; total canalicular fluorescence in these large regions was reduced approximately 2-fold in rats treated with 10 or 30 mg/kg bosentan, although the differences were not statistically significant (Table 1).

Previous studies have demonstrated that bosentan inhibits Na-dependent taurocholate uptake by suspended rat hepatocytes (Leslie et al., 2007). Consistent with these studies, our data indicated a dose-dependent inhibition of CGamF uptake by bosentan (Fig. 10, A–E), although the differences in rates were statistically significant only at a dose of 30 mg/kg. As with AMG-009, bosentan had no effect on cytosolic levels of CGamF, quantified either as cytosolic exposure from 6 to 11 minutes after injection (Fig. 10F) or as mean cytosolic fluorescence in the 9-field mosaics (Table 1).

Intravital Microscopy of the Effects of Bosentan on Hepatocyte Transport of CLF in Rats. The effects of bosentan on CLF transport essentially reproduce the effects observed on CGamF transport. As with CGamF, CLF secretion was significantly reduced in rats treated with 30 mg/kg bosentan; the rate of net secretion was reduced more than threefold (Fig. 11; Fig. 12, A and B; Table 1). The effect of bosentan on CLF secretion is also demonstrated in the 8-minute series of images shown in an accompanying video (Supplemental Video 4). The effect of bosentan on hepatocyte uptake of CLF likewise reproduces the results
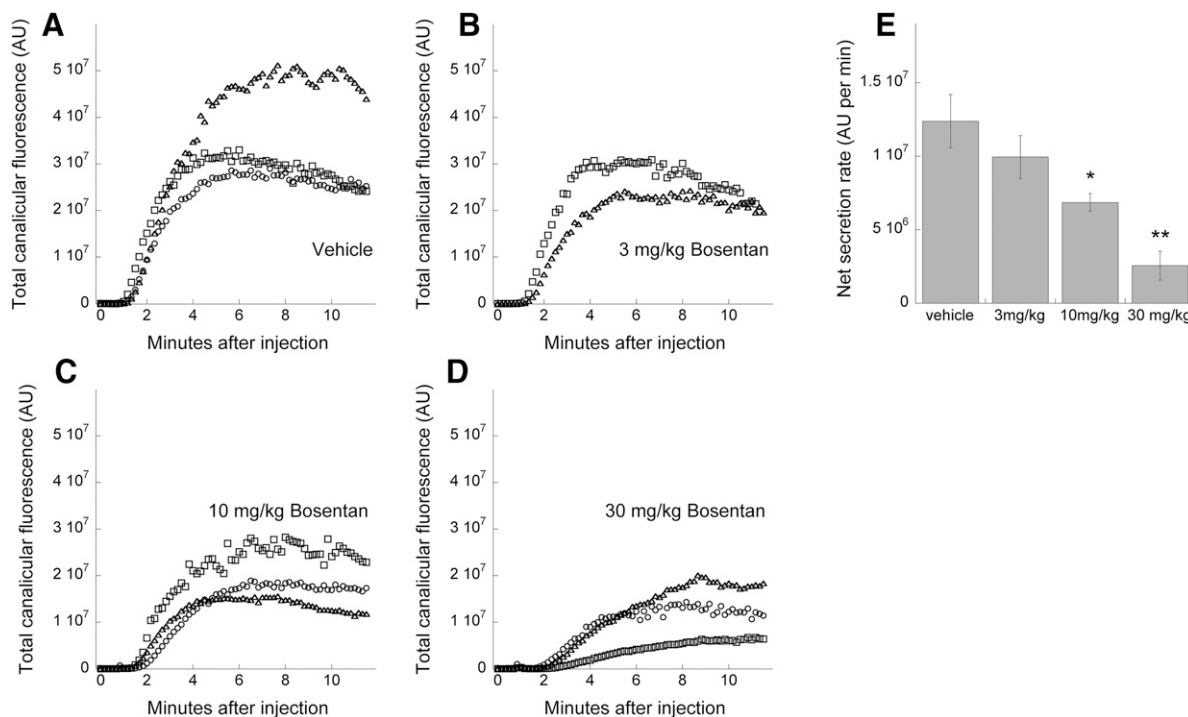
Fig. 9. In vivo dose-dependent inhibition of canalicular secretion by bosentan in rats. Kinetics of canalicular CGamF secretion for individual rats treated with (A) vehicle, (B) 3 mg/kg bosentan, (C) 10 mg/kg bosentan, or (D) 30 mg/kg bosentan. In each graph measurements are shown for each of three replicate rats, except the 3 mg/kg treatment group for which one animal was omitted due to lack of detectible bosentan in plasma. (E) Summary of effects on the rate of net CGamF secretion (linear rate during initial secretion) (mean ± S.E.M.). *$P < 0.05$; **$P < 0.01$, Dunnett's multiple comparison procedure. For all conditions, $n = 3$, except the 3 mg/kg treatment group for which one animal was omitted due to lack of detectible bosentan in plasma.

obtained with CGamF, although the effect was somewhat larger (3-fold; Fig. 12, C and D). Quantifications of cumulative cytosolic fluorescence indicate that bosentan induced a small, statistically insignificant increase in cytosolic exposure to CLF (Table 1), consistent with results obtained with CGamF.

Effects of Bosentan on Plasma Bile Acid Levels. Similar to AMG-009, 100 mg/kg intravenous administration of bosentan to rats resulted in a statistically significant elevation of total serum bile acids from 5 to 120 minutes after dose administration; bile acid levels returned to vehicle control values by 360 minutes after dose administration (Fig. 13). Animals receiving an intravenous dose of 30 mg/kg bosentan had elevated levels of serum bile acids that were statistically significant at 5, 15, and 60 minutes after dose administration, returning to control levels by 360 minutes. The dose level of 10 mg/kg bosentan had no effect on serum bile acid levels relative to vehicle controls throughout the time course.

Relative Sensitivity of the Intravital Microscopy Assay Relative to Measurement of Serum Bile Acid Levels. Our studies demonstrate that whereas the intravital microscopy assay was capable of detecting inhibitory effects of AMG-009 on CGamF secretion at doses as low as 10 mg/kg, serum bile acids were not increased at doses below 100 mg/kg. Likewise, bosentan was found to significantly inhibit CGamF secretion at doses as low as 10 mg/kg, whereas increases in serum bile acids were not apparent at doses below 30 mg/kg.

To express these differences in terms of estimated C_{max}/IC$_{50}$ ratios for Bsep and Mrp2, transport studies were conducted to measure IC$_{50}$ concentrations in inverted membrane vesicles expressing either Bsep or Mrp2. These studies (described in *Materials and Methods*) determined that AMG-009 inhibited Bsep with an IC$_{50}$ of 23 μM and inhibited Mrp2 with an IC$_{50}$ of 41 μM. In contrast, bosentan inhibited Bsep (IC$_{50}$ = 41 μM) but not Mrp2 (IC$_{50}$ > 133 μM, the highest concentration

tested). Because it was not possible to perform serial plasma sampling during the imaging procedures, C_{max} values for the intravital microscopy studies were estimated based upon plasma drug levels measured 50 minutes after drug administration. Using relationships between C_{max} and plasma concentrations obtained previously (Supplemental Fig. 3), plasma concentrations obtained for each intravital microscopy study were converted to C_{max} values by linear regression. These results are presented in Table 2, which also lists the measured plasma drug exposures for each animal.

When evaluated in terms of the estimated C_{max}/IC$_{50}$ ratios for Bsep and Mrp2, the intravital microscopy assay showed approximately 14-fold greater sensitivity to the effects of AMG-009 as compared with measurements of serum total bile acids (Table 3). Whereas significant effects of AMG-009 on serum bile acid levels were not observed at estimated C_{max}/IC$_{50}$ ratios below 44 and 25 (for Bsep and Mrp2, respectively), the intravital microscopy assay detected significant effects on CGamF secretion at estimated C_{max}/IC$_{50}$ ratios of 3.2 and 1.8, respectively.

Intravital CLF transport studies were likewise more sensitive than measurements of serum bile acids, detecting significant effects at an estimated C_{max}/IC$_{50}$ ratio of 20 (the only dose tested). The intravital microscopy assay was also more sensitive for detecting the effects of bosentan. Whereas significant effects of bosentan on serum bile acid levels were not observed at C_{max}/Bsep IC$_{50}$ ratios below 4.6, the intravital microscopy assay detected significant effects on CGamF secretion at a C_{max}/IC$_{50}$ ratio of 0.9.

Discussion

Here we describe studies in which quantitative intravital microscopy was used to characterize hepatic transport of fluorescent bile salts
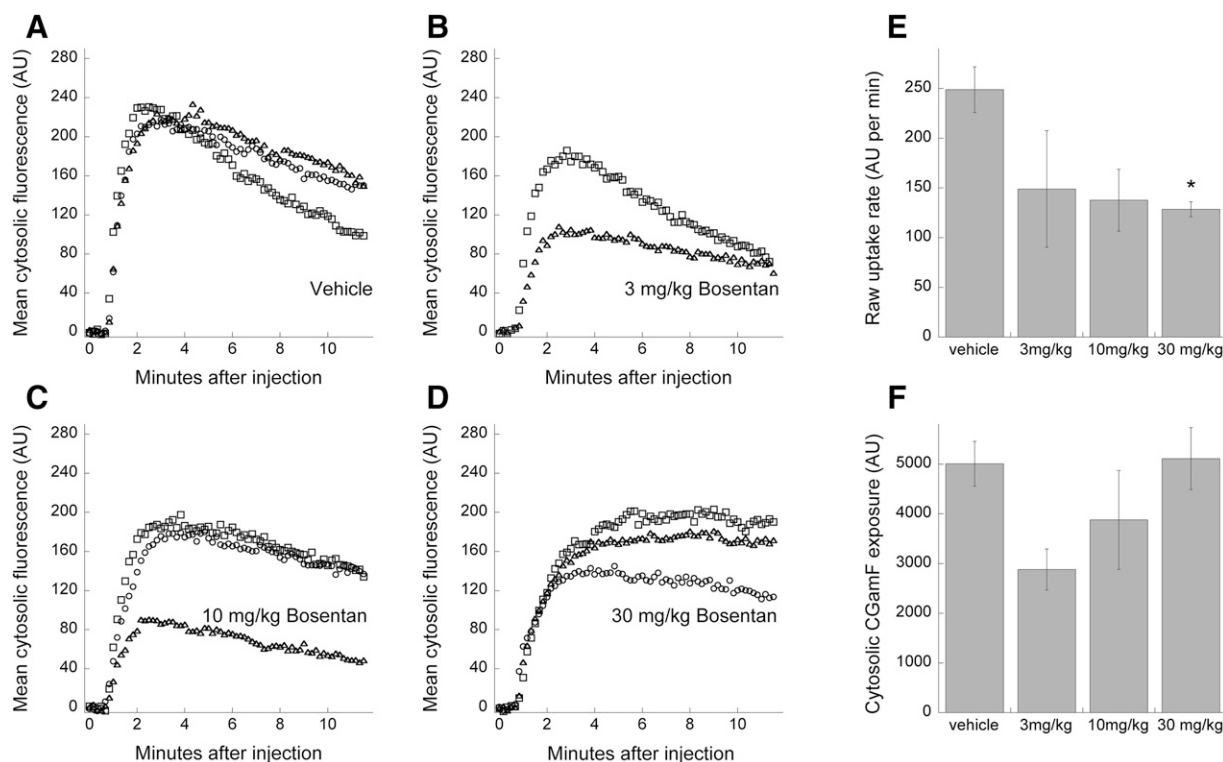
Fig. 10. Quantification of the in vivo effects of bosentan on CGamF hepatocellular uptake. Kinetics of cytosolic CGamF uptake for individual rats treated with (A) vehicle, (B) 3 mg/kg bosentan, (C) 10 mg/kg bosentan, or (D) 30 mg/kg bosentan. In each graph measurements are shown for each of three replicate rats, except the 3 mg/kg treatment group for which one animal was omitted due to lack of detectible bosentan in plasma. (E) Summary of effects on net CGamF uptake (linear rate during initial uptake). (F) Cumulative cytosolic CGamF fluorescence, measured from 6 to 11 minutes after injection of CGamF (mean ± S.E.M.). *$P < 0.05$, Dunnett's multiple comparison procedure. For all conditions $n = 3$, except the 3 mg/kg treatment group for which one animal was omitted due to lack of detectible bosentan in plasma.

CGamF and CLF, identifying dose-dependent effects of AMG-009 and bosentan on Bsep activity, two compounds associated with liver injury in humans. Although these fluorescent probes cannot represent the full spectrum of bile acids, both have been thoroughly characterized as probes of hepatic transport in rats (Boyer et al., 1994; Holzinger et al., 1997, 1998; Mills et al., 1997, 1999; Kruglov et al., 2011), whose transport is mediated by Bsep (Boyer et al., 1994; Mills et al., 1997, 1999; Kruglov et al., 2011) (Supplementary Fig. 2), indicating their appropriateness for studies of Bsep function. Although CGamF has been extensively used to characterize bile salt transport in vitro (Maglova
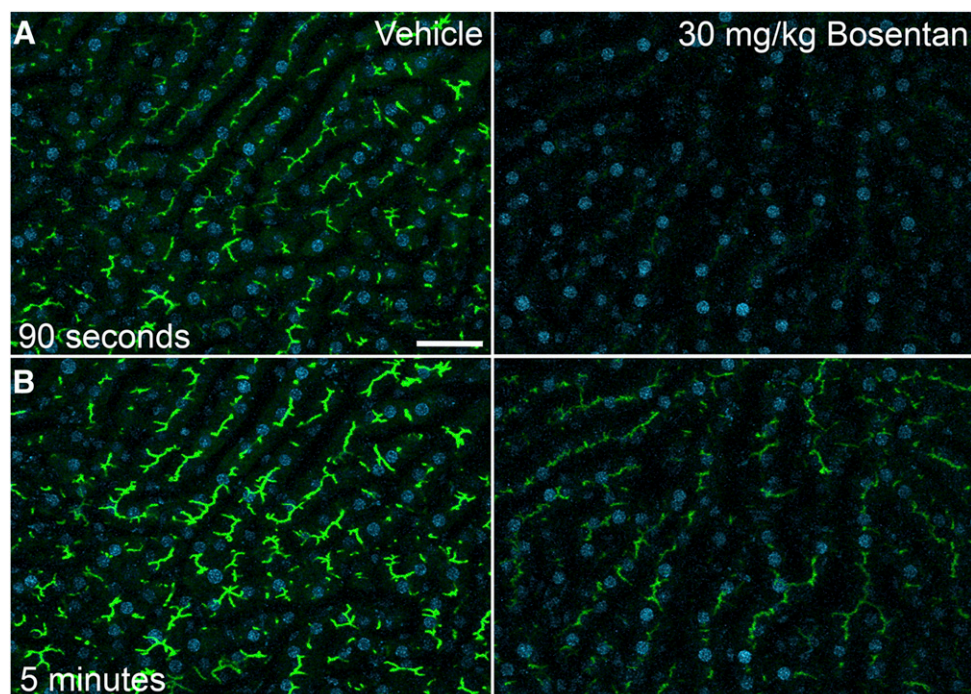

Fig. 11. Effects of bosentan on CLF transport in rat liver. Time course of CLF transport in the livers of living rats 20 minutes after intravenous injection with vehicle (left) or 30 mg/kg bosentan (right). The time-series of maximum projection (MIP) images collected over 5 minutes after intravenous injection in rats treated with vehicle or 30 mg/kg bosentan is shown in an accompanying video (Supplemental Video 4) (at ~100× speed). Scale bar is 50 μm in length.
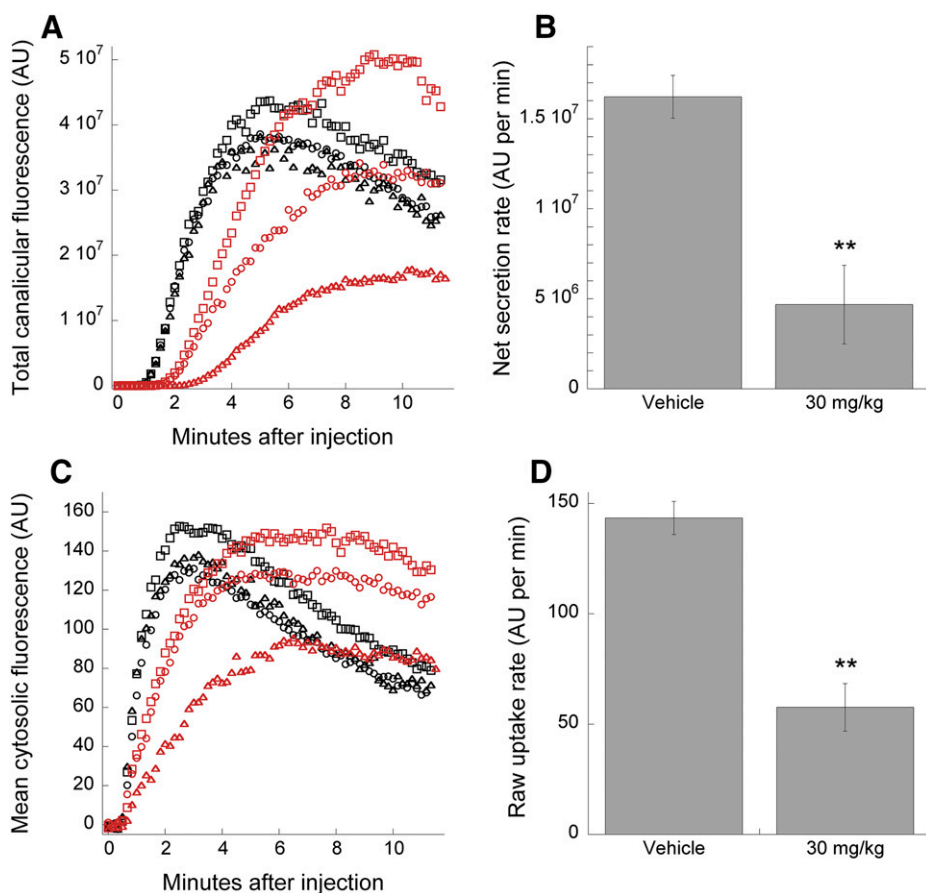
Fig. 12. Quantification of the effects of bosentan on CLF transport in vivo. (A) Kinetics of canalicular CLF secretion for individual rats treated with vehicle (black symbols) or 30 mg/kg bosentan (red symbols). Measurements are shown for each of three replicate rats for each condition. (B) Summary of effects on rates of net CLF secretion (linear rate of initial secretion), mean ± S.E.M. (C) Kinetics of cytosolic CLF uptake for individual rats treated with vehicle (black symbols) or 30 mg/kg bosentan (red symbols). Measurements are shown for each of three replicate rats for each condition. (D) Summary of effects on net CLF uptake (linear rate during initial uptake) (mean ± S.E.M.). **$P < 0.01$, Student's t test. For all conditions, $n = 3$.

et al., 1995; Cantz et al., 2000; Ye et al., 2008; Kruglov et al., 2011), the studies described here represent the first use of CGamF for intravital microscopic studies of bile acid transport and the first demonstrations of the dose-dependent effects of drugs on the individual steps of hepatocyte bile salt transport in vivo.

Quantitative analyses of images collected from living rats over time after injection of CGamF demonstrated that intravital microscopy was capable of detecting profound effects on canalicular secretion at drug dosages well below those that alter levels of serum bile acids. Whereas significant elevations of serum bile acids were not observed at doses of AMG-009 below 100 mg/kg, intravital microscopy studies demonstrated that canalicular secretion of CGamF was essentially blocked in rats treated with either 10 or 30 mg/kg, and in two out of three rats treated with 3 mg/kg. Whereas serum bile acid elevations were not observed at bosentan doses below 30 mg/kg, intravital microscopy studies detected significant decreases in canalicular secretion of CGamF at doses of 10 mg/kg.

The effects of AMG-009 and bosentan on CGamF secretion were essentially reproduced using CLF, suggesting that CLF is another useful fluorescent bile acid probe despite its lower activity as a Bsep substrate relative to CGamF (Supplemental Fig. 2). Consistent with previous studies of Mrp2-deficient TR⁻ rats (Mills et al., 1997, 1999), our intravital studies, which show that bosentan, an inhibitor of Bsep but not Mrp2, reduces CLF transport nearly 3-fold, suggest that in vivo transport of CLF is largely mediated by Bsep in rats.

The capability to resolve the hepatocyte cytosol and bile canaliculi gives intravital microscopy the unique capability to dissect hepatic transport into the component processes of hepatocyte uptake and canalicular secretion, and thus distinguish transport disruptions that could have profoundly

different consequences. These studies demonstrated that AMG-009 had no effect on the rate of CGamF uptake at any dose but reduced the rate of uptake at a dose of 30 mg/kg. In contrast, that bosentan significantly reduced the rate of uptake of both CGamF and CLF at a dose of 30 mg/kg. The basis of these different results is unclear but may reflect differences in the uptake mechanisms of CGamF and CLF.

The most striking result of these studies is that dosages of AMG-009 and bosentan sufficient to essentially block canalicular secretion did not increase cytosolic levels of CGamF and induced only modest, statistically insignificant increases in cytosolic levels of CLF. Insofar as the hepatotoxicity of Bsep inhibitors is believed to be mediated by the
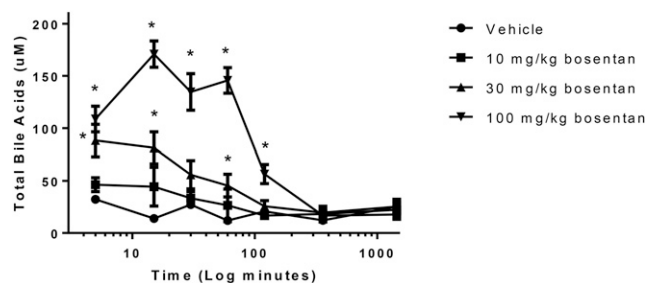
Fig. 13. Serum total bile acids in rats after a single intravenous dose of bosentan. Serum total bile acid levels in rats treated intravenously with vehicle, 10, 30, or 100 mg/kg bosentan over a 24-hour time course. Three rats per time point, per dose group. Symbols represent mean values at each time point, and bars are S.E.M. *Dunnett's post hoc comparison, $P < 0.05$ (performed in GraphPad Prism 7; GraphPad Software, San Diego, CA).

TABLE 2

Estimated drug exposure for the intravital imaging studies

Exposure of AMG-009 or bosentan during the intravital imaging studies, and an estimated C_{max} based on previously conducted intravenous studies with these compounds. As shown, subject number 1 in the 3 mg/kg bosentan dose group had no measurable exposure (limit of quantitation was 100 μg/l). Given that the other two animals in this dose group had plasma concentrations 13–36 times the limit of quantitation, it was concluded that subject number 1 was not properly dosed and imaging data for this animal was removed from the data set. The formula weight for AMG-009 is 581.47 and for bosentan is 551.62.

Compound Dose	Fluorescent Probe	Subject	Plasma	Estimated C_{max}	Estimated C_{max}	Mean Estimated C_{max}
			μg/l	μg/l	μM	μM
AMG-009						
3 mg/kg	CGamF	8	1970	3500	6	11
		9	3240	5700	10	
		10	5280	9200	16	
10 mg/kg	CGamF	11	28,600	50,000	86	74
		12	25,000	44,000	76	
		13	20,200	35,000	60	
30 mg/kg	CGamF	14	120,000	210,000	360	510
		15	191,000	330,000	570	
		16	195,000	340,000	590	
30 mg/kg	CLF	17	177,000	310,000	530	430
		18	135,000	240,000	410	
		19	115,000	200,000	350	
Bosentan						
3 mg/kg	CGamF	1	BQL	—	—	6.3
		2	1340	1900	3.4	
		3	3650	5100	9.2	
10 mg/kg[a]	CGamF	4	15,700	22,000	40	37
		5	13,800	19,000	34	
30 mg/kg[a]	CGamF	6	41,100	58,000	110	170
		7	86,700	120,000	220	
30 mg/kg	CLF	20	59,800	84,000	150	210
		21	101,000	140,000	250	
		22	88,400	120,000	220	

BQL, below the quantitation limit.
[a]Blood was not collected for exposure analysis for one animal in each of the 10 and 30 mg/kg bosentan groups.

cytosolic accumulation of bile acids (Kostrubsky et al., 2003; Morgan et al., 2010; Dawson et al., 2012), the lack of accumulation observed in our studies may explain the absence of liver injury in rats treated with AMG-009 or bosentan. More significant to the issue of drug development, our measurements of the effects of these drugs on uptake and secretion suggest potential mechanisms preventing bile acid accumulation in rats. As described here, differences in the role of these mechanisms in humans and rats may explain why these drugs cause liver injury in humans but not in rats.

The lack of cytosolic accumulation in bosentan-treated rats may reflect the fact that bosentan not only inhibited canalicular secretion but also inhibited uptake of CGamF and CLF. The effect on uptake is consistent with in vitro studies showing that bosentan inhibits rat Ntcp (Leslie et al., 2007). These same studies demonstrated that rat Ntcp is inhibited by bosentan at doses >30-fold lower than human NTCP, a difference that the investigators suggest may underlie the observation that bosentan hepatotoxicity is observed in humans but not in rats. According to this model, the accumulation of toxic bile acids that might

TABLE 3

Estimated C_{max}/transporter IC_{50} ratios relative to effects on total serum bile acid levels versus intravital imaging

Plasma was collected 50 minutes after the intravenous dose of AMG-009 or bosentan during the intravital imaging studies. C_{max} values were estimated for the intravital studies by comparing the 50-minute plasma concentrations to comparable time points from previously conducted pharmacokinetic studies in rats with AMG-009 or bosentan.

Compound Dose	C_{max} (μM, Total Drug)	C_{max}/Bsep IC_{50} Ratio	C_{max}/Mrp2 IC_{50} Ratio	Significant Effect On		
				Serum Total Bile Acids	Net Rate of CGamF Canalicular Secretion	Net Rate of CLF Canalicular Secretion
AMG-009						
3 mg/kg	11	0.48	0.27	NT	No	NT
10 mg/kg	74	3.2	1.8	No	Yes	NT
30 mg/kg[a]	470	20	11	No	Yes	Yes
100 mg/kg[b]	1010	44	25	Yes	NT	NT
Bosentan						
3 mg/kg	6.3	0.15	NC	NT	No	NT
10 mg/kg	37	0.90	NC	No	Yes	NT
30 mg/kg[a]	190	4.6	NC	Yes	Yes	Yes
100 mg/kg[b]	390	9.50	NC	Yes	NT	NT

NC, not calculated; NT, not tested.
[a]Estimated C_{max} is the mean value for the CGamF and CLF experiments.
[b]Actual mean C_{max} values from the previous studies conducted by Amgen.

occur upon Bsep inhibition in humans may be prevented in rats by a concomitant inhibition of bile acid uptake. The intravital microscopy studies presented here provide crucial support for this model, establishing that bosentan inhibits both canalicular uptake and secretion in vivo while failing to increase cytosolic levels of fluorescent bile acids even in the absence of canalicular secretion.

The absence of cytosolic accumulation of CGamF in rats treated with doses of AMG-009 sufficient to block canalicular secretion cannot be explained by effects on uptake, which we found to be completely unaffected. The lack of accumulation despite unimpeded uptake strongly suggests that the cytosolic accumulation of CGamF may be modulated by the activities of basolateral efflux transporters, such as Mrp3 or Mrp4. This interpretation is consistent with the results of studies demonstrating that taurocholate is secreted predominantly from the basolateral side of cultured rat hepatocytes (Jemnitz et al., 2010). The authors of this study suggest that basolateral secretion protects rat hepatocytes from the accumulation of Bsep substrates under conditions of Bsep inhibition. Based upon the observation that Bsep inhibition increased cytosolic taurocholate levels in human hepatocytes 25-fold beyond those observed in rat hepatocytes, they also speculated that the enhanced hepatotoxicity of Bsep inhibitors in humans may be based upon the relative weakness of this pathway in human hepatocytes.

The importance of this pathway in human hepatotoxicity of BSEP inhibitors was demonstrated in an analysis of more than 600 drugs, which showed that the ability to predict human liver injury could be increased by considering the effects on both BSEP and MRP proteins (Morgan et al., 2013). The unique window into hepatocellular transport provided by the intravital studies presented here provides critical support for this model, demonstrating that AMG-009 blocks canalicular secretion without increasing cytosolic levels of CGamF despite ongoing uptake, strongly suggesting the importance of the basolateral secretory pathway in mediating the effects of Bsep inhibitors.

A fundamental problem in pharmaceutic development is that many drugs identified as safe in studies of laboratory animals are subsequently found to induce liver injury in humans. The studies of Leslie and Jemnitz described earlier provide a template for how a thorough understanding of the effects of Bsep inhibitors on all uptake and secretory pathways may be critical to using interpreting animal studies with respect to human safety.

To the degree that the human hepatotoxicity of a BSEP inhibitor is mediated by the cytosolic accumulation of bile acids, determining the differential effects on the drug on human and rat NTCP will be crucial to identifying drugs whose human hepatotoxicity will not be predicted in studies of rats. The hepatotoxicity of BSEP inhibitors may be generally modulated in rats by a basolateral secretory pathway whose reduced activity in humans may lead to unanticipated human hepatotoxicity. Predictions of human hepatotoxicity will thus depend upon evaluation of the effects of Bsep inhibitors on the activity of both human and rat MRP transporters.

The studies presented here demonstrate how quantitative intravital microscopy can be used to provide crucial in vivo validation of these models, establishing whether in the complex in vivo setting of protein binding, metabolism, and clearance the candidate drug has the expected effects on uptake, canalicular secretion, and, crucially, cytosolic accumulation of bile acids.

Authorship Contributions

Participated in research design: Morgan, K. W. Dunn.

Conducted experiments: Ryan, Morgan, Chen, Volak.

Performed data analysis: K. W. Dunn, Morgan, Ryan, Volak.

Wrote or contributed to the writing of the manuscript: K. W. Dunn, Morgan, Ryan, Chen, Volak, R. T. Dunn.

References

Babbey CM, Ryan JC, Gill EM, Ghabril MS, Burch CR, Paulman A, and Dunn KW (2012) Quantitative intravital microscopy of hepatic transport. *IntraVital* **1**:10.

Boyer JL, Ng OC, Ananthanarayanan M, Hofmann AF, Schteingart CD, Hagenbuch B, Stieger B, and Meier PJ (1994) Expression and characterization of a functional rat liver Na⁺ bile acid cotransport system in COS-7 cells. *Am J Physiol* **266**:G382–G387.

Cantz T, Nies AT, Brom M, Hofmann AF, and Keppler D (2000) MRP2, a human conjugate export pump, is present and transports fluo 3 into apical vacuoles of Hep G2 cells. *Am J Physiol Gastrointest Liver Physiol* **278**:G522–G531.

Chen M, Suzuki A, Borlak J, Andrade RJ, and Lucena MI (2015) Drug-induced liver injury: interactions between drug properties and host factors. *J Hepatol* **63**:503–514.

Davit-Spraul A, Gonzales E, Baussan C, and Jacquemin E (2009) Progressive familial intrahepatic cholestasis. *Orphanet J Rare Dis* **4**:1.

Dawson S, Stahl S, Paul N, Barber J, and Kenna JG (2012) In vitro inhibition of the bile salt export pump correlates with risk of cholestatic drug-induced liver injury in humans. *Drug Metab Dispos* **40**:130–138.

de Waart DR, Häusler S, Vlaming ML, Kunne C, Hänggi E, Gruss HJ, Oude Elferink RP, and Stieger B (2010) Hepatic transport mechanisms of cholyl-L-lysyl-fluorescein. *J Pharmacol Exp Ther* **334**:78–86.

Dunn KW and Ryan JC (2017) Using quantitative intravital multiphoton microscopy to dissect hepatic transport in rats. *Methods* **128**:40–51.

Fattinger K, Funk C, Pantze M, Weber C, Reichen J, Stieger B, and Meier PJ (2001) The endothelin antagonist bosentan inhibits the canalicular bile salt export pump: a potential mechanism for hepatic adverse reactions. *Clin Pharmacol Ther* **69**:223–231.

Feng B, Xu JJ, Bi YA, Mireles R, Davidson R, Duignan DB, Campbell S, Kostrubsky VE, Dunn MC, Smith AR, and Wang HF (2009) Role of hepatic transporters in the disposition and hepatotoxicity of a HER2 tyrosine kinase inhibitor CP-724,714. *Toxicol Sci* **108**:492–500.

Fouassier L, Kinnman N, Lefèvre G, Lasnier E, Rey C, Poupon R, Elferink RP, and Housset C (2002) Contribution of mrp2 in alterations of canalicular bile formation by the endothelin antagonist bosentan. *J Hepatol* **37**:184–191.

Funk C, Pantze M, Jehle L, Ponelle C, Scheuermann G, Lazendic M, and Gasser R (2001a) Troglitazone-induced intrahepatic cholestasis by an interference with the hepatobiliary export of bile acids in male and female rats. Correlation with the gender difference in troglitazone sulfate formation and the inhibition of the canalicular bile salt export pump (Bsep) by troglitazone and troglitazone sulfate. *Toxicology* **167**:83–98.

Funk C, Ponelle C, Scheuermann G, and Pantze M (2001b) Cholestatic potential of troglitazone as a possible factor contributing to troglitazone-induced hepatotoxicity: in vivo and in vitro interaction at the canalicular bile salt export pump (Bsep) in the rat. *Mol Pharmacol* **59**:627–635.

Holzinger F, Schteingart CD, Ton-Nu HT, Cerre C, Steinbach JH, Yeh HZ, and Hofmann AF (1998) Transport of fluorescent bile acids by the isolated perfused rat liver: kinetics, sequestration, and mobilization. *Hepatology* **28**:510–520.

Holzinger F, Schteingart CD, Ton-Nu HT, Eming SA, Monte MJ, Hagey LR, and Hofmann AF (1997) Fluorescent bile acid derivatives: relationship between chemical structure and hepatic and intestinal transport in the rat. *Hepatology* **26**:1263–1271.

Jemnitz K, Veres Z, and Vereczkey L (2010) Contribution of high basolateral bile salt efflux to the lack of hepatotoxicity in rat in response to drugs inducing cholestasis in human. *Toxicol Sci* **115**:80–88.

Kostrubsky VE, Strom SC, Hanson J, Urda E, Rose K, Burliegh J, Zocharski P, Cai H, Sinclair JF, and Sahi J (2003) Evaluation of hepatotoxic potential of drugs by inhibition of bile-acid transport in cultured primary human hepatocytes and intact rats. *Toxicol Sci* **76**:220–228.

Kostrubsky SE, Strom SC, Kalgutkar AS, Kulkarni S, Atherton J, Mireles R, Feng B, Kubik R, Hanson J, Urda E, and Mutlib AE (2006) Inhibition of hepatobiliary transport as a predictive method for clinical hepatotoxicity of nefazodone. *Toxicol Sci* **90**:451–459.

Kruglov EA, Gautam S, Guerra MT, and Nathanson MH (2011) Type 2 inositol 1,4,5-trisphosphate receptor modulates bile salt export pump activity in rat hepatocytes. *Hepatology* **54**:1790–1799.

Leslie EM, Watkins PB, Kim RB, and Brouwer KL (2007) Differential inhibition of rat and human Na⁺-dependent taurocholate cotransporting polypeptide (NTCP/SLC10A1)by bosentan: a mechanism for species differences in hepatotoxicity. *J Pharmacol Exp Ther* **321**:1170–1178.

Letzsch S, Boettcher K, Kelm J, and Messner S (2015) Quantifying efflux activity in 3D liver spheroids. *Genet Eng Biotechnol News* **35**:2.

Maglova LM, Jackson AM, Meng XJ, Carruth MW, Schteingart CD, Ton-Nu HT, Hofmann AF, and Weinman SA (1995) Transport characteristics of three fluorescent conjugated bile acid analogs in isolated rat hepatocytes and couplets. *Hepatology* **22**:637–647.

Maxfield FR and Dunn KW (1990) Studies of endocytosis using image intensification fluorescence microscopy and digital image analysis, in *Optical Microscopy for Biology* (Jacobsen K ed) pp 357–371, Alan Liss, New York.

Mills CO, Milkiewicz P, Müller M, Roma MG, Havinga R, Coleman R, Kuipers F, Jansen PL, and Elias E (1999) Different pathways of canalicular secretion of sulfated and non-sulfated fluorescent bile acids: a study in isolated hepatocyte couplets and TR⁻ rats. *J Hepatol* **31**:678–684.

Mills CO, Milkiewicz P, Saraswat V, and Elias E (1997) Cholyllysyl fluroscein and related lysyl fluorescein conjugated bile acid analogues. *Yale J Biol Med* **70**:447–457.

Mita S, Suzuki H, Akita H, Hayashi H, Onuki R, Hofmann AF, and Sugiyama Y (2006) Inhibition of bile acid transport across Na⁺/taurocholate cotransporting polypeptide (SLC10A1) and bile salt export pump (ABCB 11)-coexpressing LLC-PK1 cells by cholestasis-inducing drugs. *Drug Metab Dispos* **34**:1575–1581.

Morgan RE, Trauner M, van Staden CJ, Lee PH, Ramachandran B, Eschenberg M, Afshari CA, Qualls CW, Jr, Lightfoot-Dunn R, and Hamadeh HK (2010) Interference with bile salt export pump function is a susceptibility factor for human liver injury in drug development. *Toxicol Sci* **118**:485–500.

Morgan RE, van Staden CJ, Chen Y, Kalyanaraman N, Kalanzi J, Dunn RT, 2nd, Afshari CA, and Hamadeh HK (2013) A multifactorial approach to hepatobiliary transporter assessment enables improved therapeutic compound development. *Toxicol Sci* **136**: 216–241.

National Research Council (NRC). (2011) *Guide for the Care and Use of Laboratory Animals*. 8th ed. National Academies Press, Washington, DC, http://grants.nih.gov/grants/olaw/Guide-for-the-care-and-use-of-laboratory-animals.pdf.

Olson H, Betton G, Robinson D, Thomas K, Monro A, Kolaja G, Lilly P, Sanders J, Sipes G, Bracken W, et al. (2000) Concordance of the toxicity of pharmaceuticals in humans and in animals. *Regul Toxicol Pharmacol* **32**:56–67.

Ryan JC, Dunn KW, and Decker BS (2014) Effects of chronic kidney disease on liver transport: quantitative intravital microscopy of fluorescein transport in the rat liver. *Am J Physiol Regul Integr Comp Physiol* **307**:R1488–R1492.

Stieger B, Meier Y, and Meier PJ (2007) The bile salt export pump. *Pflugers Arch* **453**:611–620.

Swift B, Pfeifer ND, and Brouwer KL (2010) Sandwich-cultured hepatocytes: an in vitro model to evaluate hepatobiliary transporter-based drug interactions and hepatotoxicity. *Drug Metab Rev* **42**:446–471.

van Staden CJ, Morgan RE, Ramachandran B, Chen Y, Lee PH, and Hamadeh HK (2012) Membrane vesicle ABC transporter assays for drug safety assessment. *Curr Protoc Toxicol* **Chapter 23**:Unit 23 25.

Wang R, Chen HL, Liu L, Sheps JA, Phillips MJ, and Ling V (2009) Compensatory role of P-glycoproteins in knockout mice lacking the bile salt export pump. *Hepatology* **50**:948–956.

Woodhead JL, Yang K, Siler SQ, Watkins PB, Brouwer KL, Barton HA, and Howell BA (2014) Exploring BSEP inhibition-mediated toxicity with a mechanistic model of drug-induced liver injury. *Front Pharmacol* **5**:240.

Ye ZW, Augustijns P, and Annaert P (2008) Cellular accumulation of cholyl-glycylamido-fluorescein in sandwich-cultured rat hepatocytes: kinetic characterization, transport mechanisms, and effect of human immunodeficiency virus protease inhibitors. *Drug Metab Dispos* **36**: 1315–1321.

Address correspondence to: Ryan E. Morgan, Amgen Inc., Department of Comparative Biology and Safety Sciences, One Amgen Center Dr., 29-2-A, Thousand Oaks, CA 91320. E-mail: remorgan@amgen.com; or Dr. Kenneth W. Dunn, Indiana University Medical Center, Department of Medicine, Division of Nephrology, 950 W. Walnut St., RII-202B, Indianapolis, Indiana 46202-5116. E-mail: kwdunn@iu.edu